Welding International
Vol. 24, No. 10, October 2010, 739–748
Selected from *Soldagem & Inspeção* 2009 14(2) 104–113

Taylor & Francis
Taylor & Francis Group

Microstructure development in Nd:YAG laser welding of AISI 304 and Inconel 600

Maurício David M. das Neves[a1], André Lotto[b], José Roberto Berretta[c], Wagner de Rossi[d] and Nilson Dias V. Júnior[d]

[a]*Institute of Energy and Nuclear Research – IPEN CNEN/SP, Centre of Science and Materials Technology (CCTM), São Paulo, São Paulo State, Brazil;* [b]*University Centre of the Faculty of Industrial Engineering of S. B. C., São Paulo, São Paulo State, Brazil;* [c]*CTMSP – Centre of Naval Technology in São Paulo, São Paulo, São Paulo State, Brazil;* [d]*Institute of Energy and Nuclear Research, Centre for Lasers and Applications (CLA), São Paulo, São Paulo State, Brazil*

(*Received 9 April 2008; final version received 2 February 2009*)

In this work, the morphology of solidification of the weld zone (WZ) was studied in a joint formed from dissimilar materials, composed of austenitic AISI 304 stainless steel and Inconel 600 nickel alloy, welded with an Nd:YAG-pulsed laser. The laser beam and optical system parameters were selected with a view to obtain a weld with total penetration and good surface finish. The microstructural characterization was carried out using an optical microscope, in which a WZ was seen with total penetration, keyhole-type, presence of small pores and absence of cracks. The welded joints were also characterized by means of an electron scan microscope. Measurements taken by X-ray spectrometry for dispersion of the energy in the WZ indicated a slightly heterogeneous distribution of nickel and iron. It was seen that the start of solidification in the WZ occurred by means of epitaxial growth. The morphology of WZ solidification was basically denditric and cellular, being influenced by the temperature gradient, solidification speed and chemical composition. The variations in chemical composition and solidification morphology do not significantly alter the Vickers microhardness values in the WZ. Results obtained in the tensile tests indicate suitably effective welding values.

Keywords: laser welding using Nd:YAG; stainless steel AISI 304; Inconel 600; dissimilar materials

1. Introduction

Diverse welding applications for dissimilar materials using the interface between stainless steel AISI 304 and Inconel 600 have been developed in various industrial sectors[1]. The recent use of apogee motors installed in artificial satellites has generated an increasing demand for injectors that are highly reliable, low weight and have reduced energy consumption. These injectors, as can be seen in Figure 1, must have excellent watertight integrity, high dimensional precision and great geometric complexity and, therefore, must be produced by using a welding technique that gives a small heat-affected zone (HAZ).

Pressure sensors with different geometries are used in chemical and petrochemical plants, with the objective of controlling flows, pressures and other parameters, in pipes and storage tanks. The basic function of these sensors is to provide information about the processes, facilitating their automation. Weld sealing is a critical manufacturing stage and must take place without any great distortion. These joints, which are normally of dissimilar materials, must have high integrity and be able to cope with aggressive conditions. Nuclear power plants that use pipes with Inconel and stainless steel interfaces must also be joined by processes that enable a reduced HAZ and little presence of residual stresses.

The use of laser welding for these and other applications[2,3] has grown in recent years, since the process enables accurate welds, a high penetration/bead width, a small HAZ and reduced distortion of the base materials (BMs).

The welding of similar or dissimilar BMs using the laser process forms a region known as the weld zone (WZ). In the case of welding dissimilar materials, differences in chemical composition of the WZ may cause, in service, mechanical and metallurgical behaviour that is different from the BMs. Some factors may be responsible for faults in these welds, such as the formation of fragile phases and limited solubility of an alloy constituent or phase, differences in the fusion points, distinct thermal conductivity, initial characterization of WZ solidification (epitaxial growth) and alterations in the solidification morphology[4].

The WZ solidification process occurs by the mechanisms of nucleation and growth of new phases, starting from a solid–liquid interface. The start of solidification of the WZ can take place in three distinct ways, respectively, homogenous nucleation, heterogeneous nucleation and epitaxial growth. Figure 2 shows schematically the various ways that a WZ can start to grow. The form of growth in the solid phase of the WZ is connected to the surface tensions in both the liquid and solid, as can be seen in Figure 3, which determine the malleability angle (θ), see Equation (1). With no malleability or with a malleability angle (θ) close to 180°, homogenous nucleation occurs: this is the rarest type

ISSN 0950-7116 print/ISSN 1754-2138 online

DOI: 10.1080/09507110903568877
http://www.informaworld.com

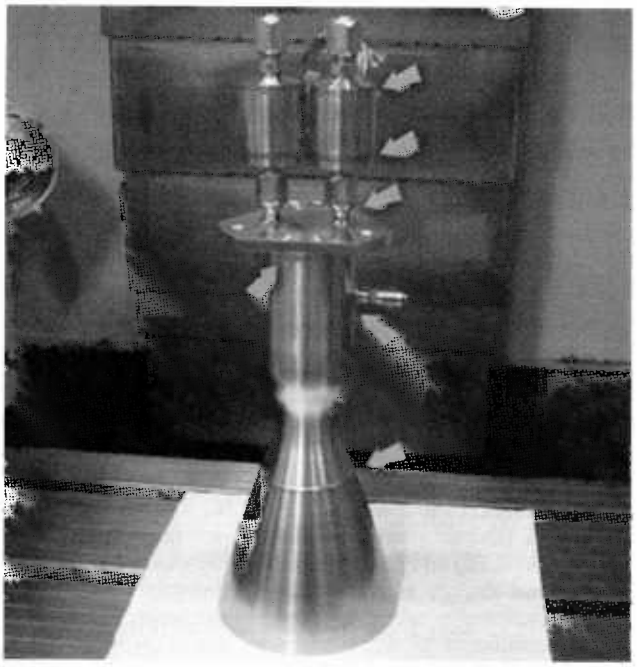

Figure 1. Prototype of the propulsion mechanism to guide the Brazilian satellite, and the location of the joints made on its external surface. Welds are indicated by arrows and produced at the Institute of Energy and Nuclear research – CLA.

of growth and requires high levels of super-cooling. When the malleability angle is close to 90°, heterogeneous nucleation occurs, that is, a solid surface acts as the solidification nucleus for the liquid in contact[4]. A malleability angle close to 0°, in other words total malleability, induces epitaxial growth, where the activation energy is practically zero and super-cooling is not necessary.

In this form of solidification, the solid surfaces are formed to a lesser extent and therefore less energy is needed in comparison with those mentioned above (homogenous and heterogeneous nucleation). The atoms adhere to the existing sub-stratum, encouraging its growth. This type of solidification occurs normally when a liquid solidifies on a sub-stratum that has a similar chemical composition and crystalline structure, as can be seen in welds[5,6].

The start of WZ solidification when welding similar BMs occurs by means of epitaxial growth. When welding dissimilar materials, the start of WZ solidification may occur by means of epitaxial growth. Various studies into welding of dissimilar BMs confirm that the start of WZ solidification occurs by means of epitaxial growth, starting with the sub-stratum (solid) and proceeding by means of competitive growth of the grains in the direction of the central region of the weld[7–10].

Epitaxial growth is a phenomenon in which the grains in the WZ grow with the same crystalline orientation as the grains in the HAZ. The motive force needed for the nucleation of new grains is low, since the thermodynamic barrier to solidification is practically eliminated. As a result, each one of these new grains solidified in the same crystallographic direction as the grains in the HAZ. This reduction in free energy is a consequence of the reduction in interface energy, which is effectively achieved if the solid is formed on another surface with a similar crystalline orientation, as with epitaxial growth[11–13].

After the start of solidification in the direction of the centre of the WZ, the growth in grains follows a direction parallel to the maximum temperature gradient, encouraging competitive growth of grains. Those grains with an orientation favourable to the direction of the maximum temperature gradient show higher growth when compared with grains that run in less favourable directions. The preferential growth direction for cubic materials with a centred part (CCC) and cubic materials with a centred phase (CFC) is $<100>$[5,14,15]. Figure 4 shows schematically the presence of both epitaxial growth and competitive growth of the grains.

Epitaxial growth is beneficial to the welds, since it enables the WZ to have continuity in the grains from the base metal. This therefore prevents the connection zone (CZ) (the WZ–HAZ interface) becoming a region with a concentration of stresses. Normally when welding, the surfaces are cleaned to facilitate the liquid metal's adherence to the BMs. The consequence is a greater interaction between the BMs and the liquid metal in the WZ. The morphology of solidification in the WZ is basically controlled by the degree of constitutional supercooling, which depends on the heat gradient, solidification speed and concentration of solute in the solid–liquid phase (S-L). The heat gradient (G) is the variation in temperature in the liquid in relation to distance, starting from the solid–liquid interface (S-L). The solidification

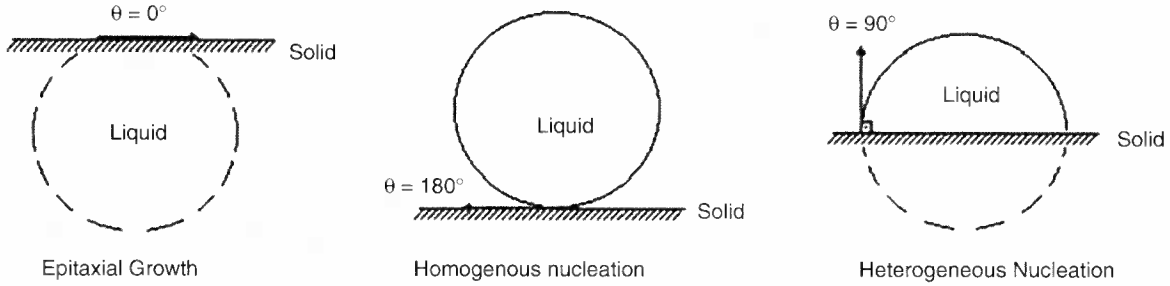

Figure 2. Schematic representation of the growth forms of a solid from a liquid phase.

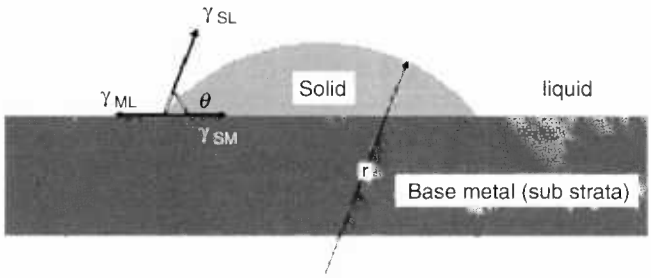

Figure 3. Schematic representation of surface stresses of the phases (solid and liquid) and malleability[4].

speed (R) is related to the advance in the solid–liquid interface and this in turn depends on the variation in the liquid temperature[4],

$$\gamma_{LM} = \gamma_{SM} + \gamma_{SL} \cdot \cos\theta \quad \cos\theta = \frac{(\gamma_{ML} - \gamma_{SM})}{\gamma_{SL}}. \quad (1)$$

γ_{LM}, Liquid – Metal surface tension; γ_{SM}, Solid – Metal surface tension; γ_{SL}, Solid – Liquid surface tension; θ, angle of malleability.

Constitutional super-cooling occurs in the solidification of an alloy, as a result of the chemical composition of the solid phase being different from the chemical composition of the liquid phase. The solubility of the solute in the solid phase is less than that in the liquid phase. As a result, there is a concentration gradient for the solute from the solid–liquid interface to the liquid metal. The variation in concentration causes a reduction in liquid temperature, facilitating solidification in one direction, contributing to constitutional super-cooling from the interface (S-L).

Different solidification modes may occur in the WZ, such as plane, cellular, dendritic cellular, dendritic columnar and equiaxial dendritic. Figure 5(a) represents schematically the various growth morphologies in relation to the temperature gradient imposed on the cooling (G) and the advance speed of the solid–liquid interface (R).

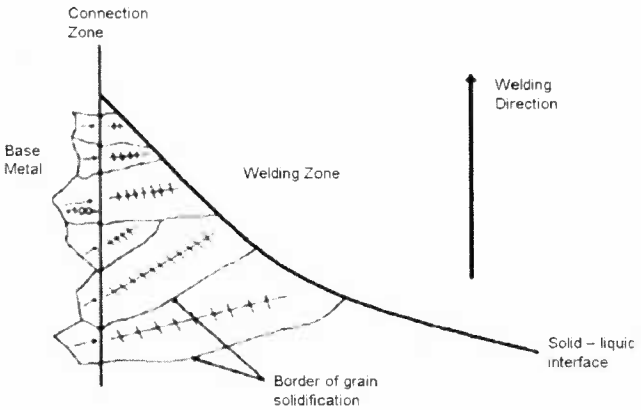

Figure 4. Schematic representation of the epitaxial growth and competitive growth of grains in the WZ[13].

A gradual increase in constitutional super-cooling can be seen, represented by the area between the 'liquidus' line (the 'liquidus' temperature) and the line of the heat gradient imposed, in relation to the reduction in the heat gradient, as shown in Figure 5(b). During plane growth, constitutional super-cooling is practically zero, and its value will increase from cellular growth to dendritic. Low values of R and high values of G, as occur at the start of

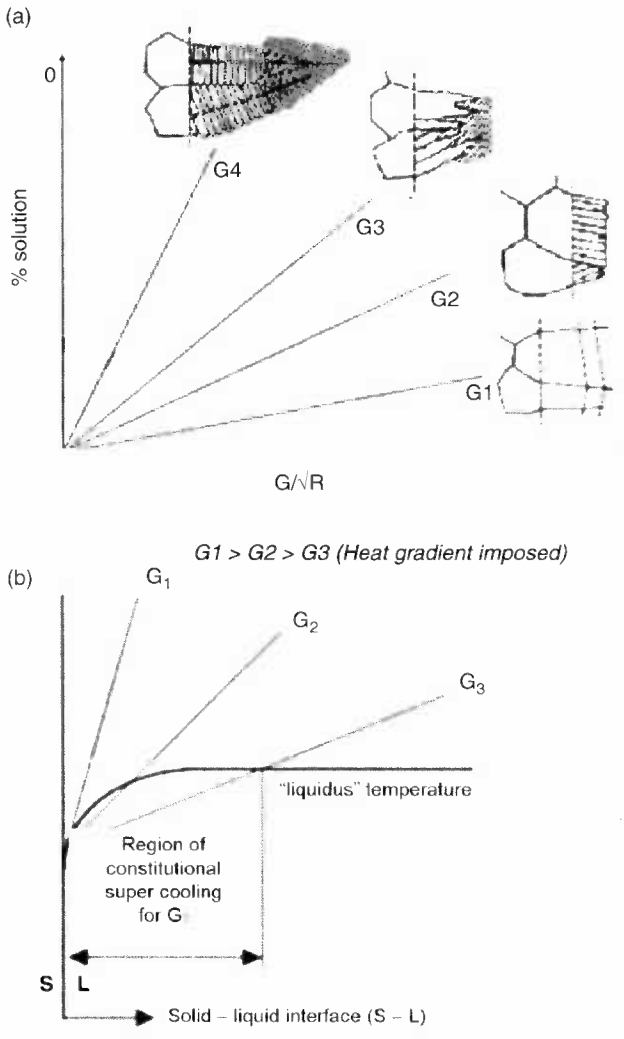

Figure 5. (a) Schematic representation of the different modes of solidification for the $G/\sqrt{R}$ and (b) constitutional super-cooling region in relation to the heating gradient[13].

solidification, favour a planar solidification morphology for the S-L interface[8]. As the front advances towards the centre of the WZ, the value of R rises rapidly, resulting in a transition from planar morphology to cellular or dendritic. Each grain has a single crystallographic orientation, which coincides with the direction of the main dendritic axis[16].

The G/R ratio shown in Figure 5(a) is used to study the solidification mode. A low value for this ratio means that the liquid is constitutionally super-cooled and the dendritic growth of the interface is stable for a given percentage of solute. On the other hand, for high values, the liquid is not constitutionally super-cooled and encourages plane growth in the interface. The increase in temperature gradient (G) is related to the reduction in the constitutionally super-cooled region, favouring plane growth. When the gradient is reduced, the super-cooled region is larger and the trend is to encourage dendritic growth, as represented in Figure 5(a),(b).

The high energy densities supplied by the laser beam generate high temperature gradients, in the order of 105–107 K/m, which allow high welding speeds to be used (1 to 100 mm/s). Studies carried out in these conditions indicate that the solidification morphologies of AISI 304[16–18] and of Inconel 600[19,20] must be denditric or cellular-denditric and the HAZ must be totally austenitic. The laser process has a high concentration of energy, and therefore the R and G parameters are raised. The G/R ratio that indicates the cooling speed of the WZ has a high value, favouring solidification with a fine microstructure and can lead to better mechanical properties in these welded regions[15,16].

The objective of this work is to study the microstructural and mechanical characteristics of the regions known as the WZ and the CZ in welding with a pulsed Nd:YAG laser between austenitic AISI 304 stainless steel and Inconel 600 alloy.

2. Materials and methods

2.1 Materials

The chemical compositions of the BMs are shown in Table 1.

2.2 Methodology

The welds in the materials were produced using equipment developed in the Institute of Nuclear and Energy Research (IPEN), known as the Laser Material Processing Centre. The laser used was an Nd:YAG, pulsed, with an energy level per pulse of up to 10 J, a highest repetition rate of 300 Hz, average power of 100 W and peak power of 3 KW. The samples were prepared from plates that were 0.8 mm thick, cut into 20 × 50 mm rectangles. The materials were welded and fitted into a device developed as shown in Figure 6, to help with positioning and fixing. The BM joints were top welds with a gap close to zero.

The laser parameters were energy (E) = 6.0, average power (Pm) = 84 W, pulse time (tp) = 7 ms (7.10^{-3} s) and frequency (f) = 14 Hz. The laser beam was focused using a lens of focal length (f) of 100 mm, and the focal point was located 3 mm below the surface of the BMs, therefore, for one of the BMs. The weld beads were produced in a single pass, with welding speed (v) = 300 mm/min (5 mm/s) and 30% partial overlapping of the pulses[1]. A gaseous argon mix (10 l/min) was used sprayed from a nozzle with 6 mm diameter, concentric with the bead and 4 mm away from the surfaces.

The welded samples were cut along the transversal and longitudinal sections. After the metallographic preparation and electrochemical attack, the samples were characterized by optical microscope (MO) and electron scan microscope (ESM). Characterization by MO took place in the Powder Metallurgy laboratory of IPEN and in the Materials Laboratory of the Central University of the Faculty of Industrial Engineering (FEI). An ESM (a Philips XL 30) at IPEN was used to observe the WZ/HAZ interface and verify the distribution of the elements (Fe, Cr and Ni) in the WZ. The Vickers microhardness profile, in relation to distance was used in Shimatzu equipment located in the FEI. The measurements were taken with a load of 40 g on the surface of the sample, with positioning similar to that for X-ray spectrometry analysis for energy dispersion (EDX). Tensile tests were carried out and the welding efficiency was calculated as a percentage, being the quotient between the breaking load of the welded joint over the breaking load of the BM.

3. Results and discussion

The analyses made using an MO of the section of the weld beads are shown in Figures 7 and 8. Figure 7(a) shows an image that is characteristic of the geometry of the cross section of the WZ. In the conditions employed in this study, total penetration of welding can be seen, with typical 'keyhole' geometry, in other words a high depth/width ratio. Figure 7(b) shows distribution profiles of the elements in the WZ, when the laser beam (L) is positioned in the joint (J). Concentration gradients were seen in the WZ, in particular, nickel and iron, as a

Table 1. Chemical composition of the BMs used.

	Ni (%)	Cr (%)	Fe (%)	C (%)	Mn (%)	Si (%)	S (%)	P (%)	Mo (%)	Cu (%
AISI 304	8.9	18.4	71.2	0.07	1.06	0.34	–	0.03	0.05	0.03
Inconel 600	74.9	14.9	9.4	0.01	0.27	0.27	0.04	–	–	0.21

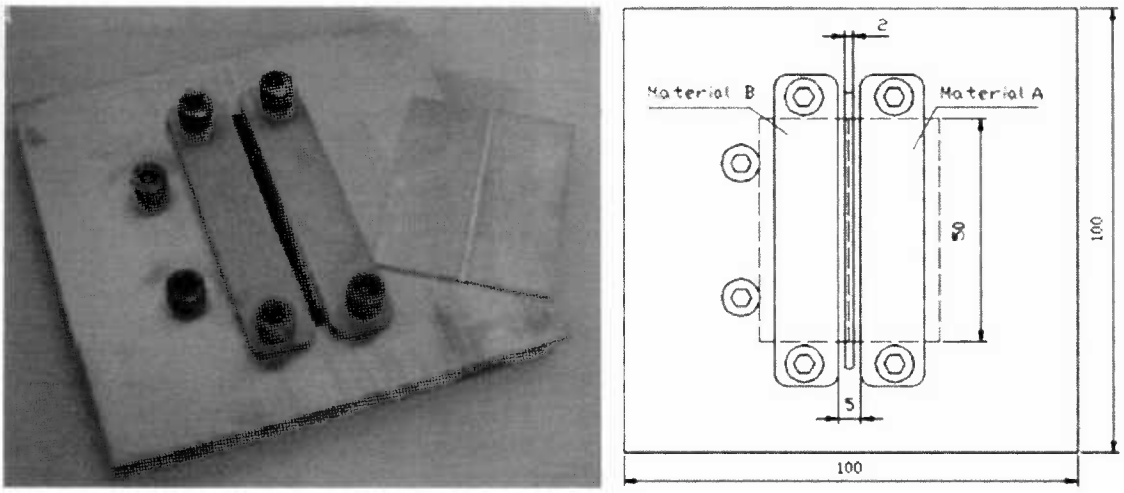

Figure 6. Device developed to fix and weld the base metals.

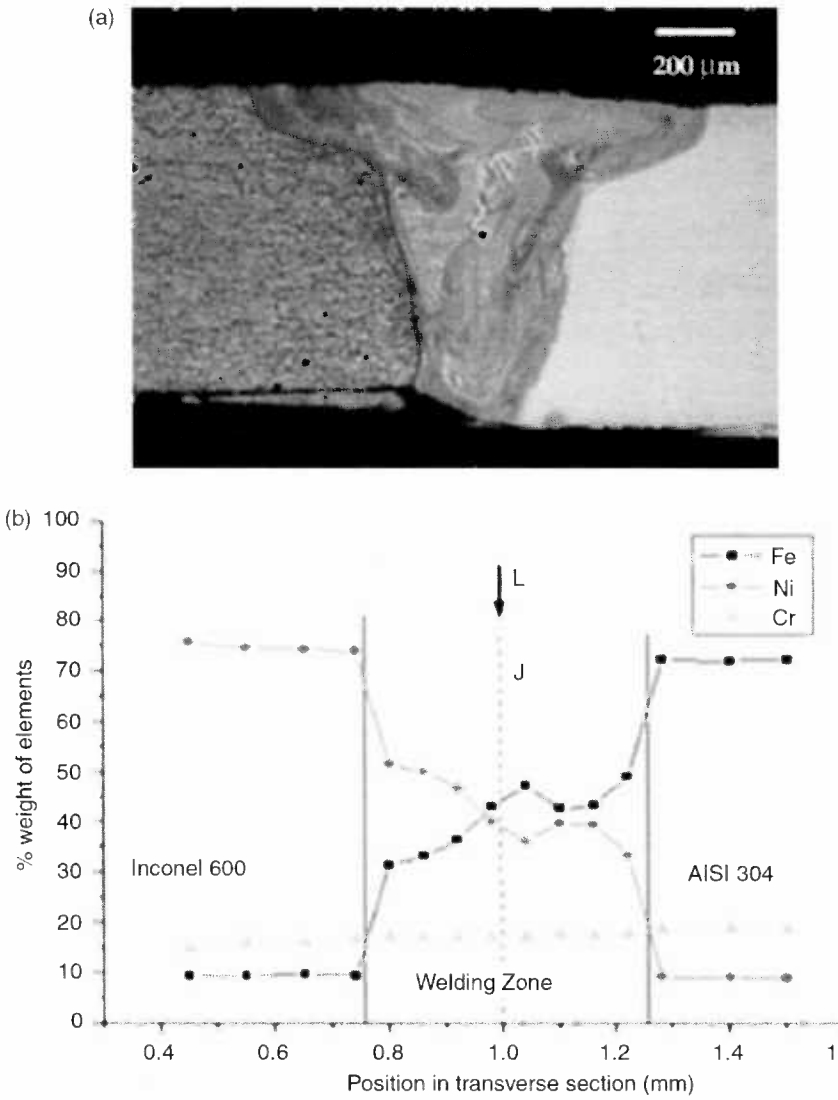

Figure 7. (a) Image obtained under an MO for the WZ of the cross section with a laser beam (arrow L) incidental on the joint (J – dotted line) and (b) graph of % weight of the elements (Fe, Ni and Cr) extracted from the reference[1].

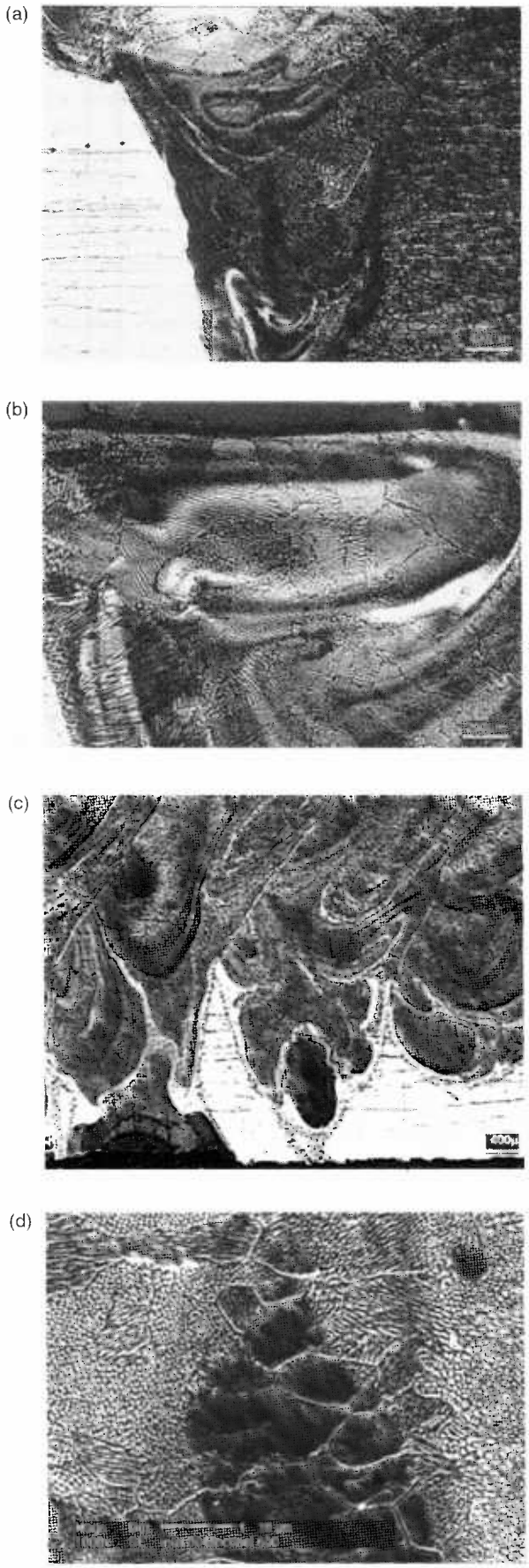

Figure 8. Images obtained under a microscope for the WZ; optical (a), (b) and (c) and electron scan (d).

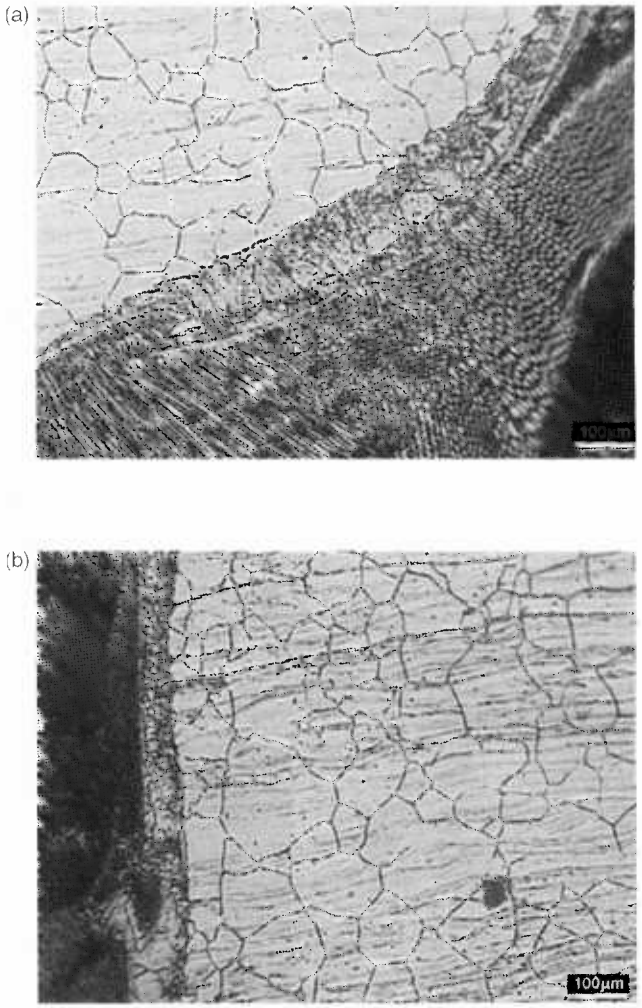

Figure 9. (a) and (b) Images obtained under an MO for the WZ interface and stainless steel (CZ).

consequence of the differences in the chemical composition of the BMs. The distribution of the nickel and iron elements are reasonably homogenous in the central region of the WZ, while close to the interface there are greater differences in composition.

Figure 8(a),(b),(c) shows the MO results and Figure 8(d) shows the ESM results, confirming that the microstructure of the WZ is fine, as a consequence of the high solidification and cooling speed, being generated by the high rate of heat extraction from the welded joint. Small pores can be seen that are smaller than 20 µm (20×10^{-6} m), attributed to keyhole penetration. No cracks are seen in the WZ, regardless of whether the region analysed is close to the interface with the AISI 304 or with the Inconel 600.

Figure 8(c),(d) shows images of longitudinal sections of the WZ. Penetration of the weld is total and homogenous, despite Figure 8(c) suggesting a heterogeneous penetration. This effect is caused by the inclined cut of the analysed section to facilitate observation of the region where total penetration takes place.

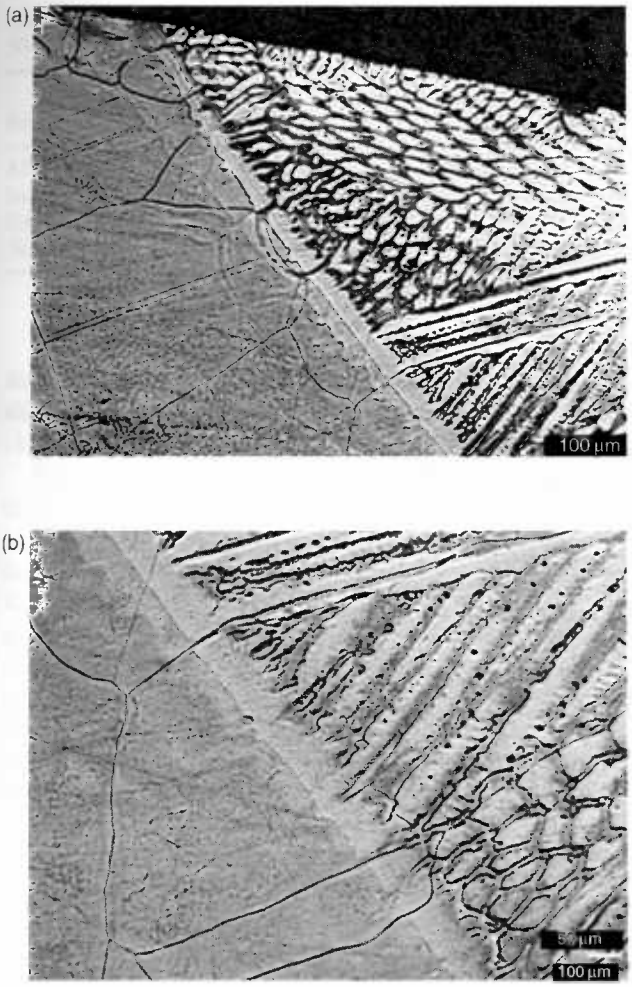

Figure 10. (a) and (b) Images obtained under an MO for the interface between the WZ and the Inconel 600.

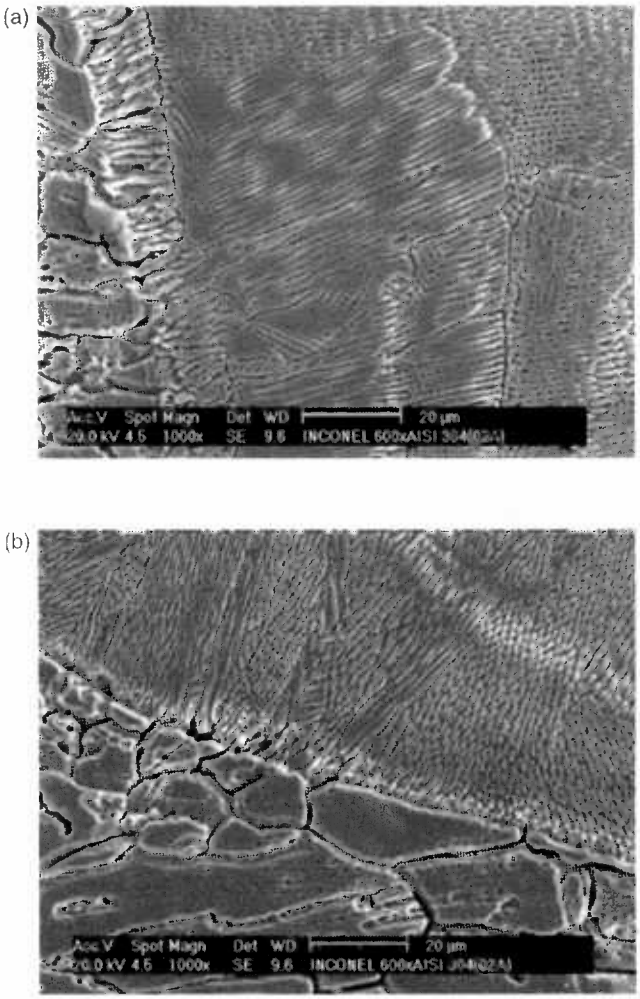

Figure 11. (a) and (b) Images obtained by ESM for the interface between the WZ and the AISI 304 stainless steel.

It can be seen that the point overlapping obtained by the laser beam pulses is uniform in the conditions employed.

Figures 9 and 10 show the images obtained by MO and Figures 11 and 12 show the images obtained by ESM. The majority of these images show the WZ/HAZ interface, also known as the CZ. Note that solidification of the weld bead starts with the epitaxial growth of the grains in the partially WZ, throughout the solid–liquid interface, as can be verified in Figures 9–12. The liquid metal of the WZ solidifies, forming a continuation of the grains in the base metal. Despite the difference in chemical composition, as in Figure 7(b), evidence can be seen for epitaxial growth, that is, there is no loss of correlation between the direction of the new grains in the WZ with the grains in the BMs.

In the WZ, a low solidification speed and a high temperature gradient at the start of WZ encourage a plane solidification front. After the initial solidification, the S-L interface advances towards the centre and the solidification speed increases, in relation to the start of WZ solidification, resulting in a transition in the front from plane solidification to cellular, cellular-dendritic or dendritic.

Note that each grain in the WZ has a crystallographic orientation, which coincides with the orientation of the dendrites or cells, as seen in Figures 9–12. The dendrites that have the lowest angle between the main axle and the direction of the highest temperature gradient have the highest speed of growth and prevent the growth of other grains, in particular, those that do not have a favourable orientation.

The start of WZ growth occurs in an epitaxial way, and therefore it is important for the HAZ grains to be smaller, to generate larger grains in the WZ.

Epitaxial growth is beneficial to the weld, since it provides continuity to the grains in the BMs, reducing the regions in the welds that have stress concentrations, in particular, cracks[16].

The typical WZ microstructure is shown in Figure 13. It can be seen that the WZ solidification morphology is basically denditric in the areas of greatest pulse depth, as in the lower parts of Figure 13. For location where the passes are not so deep, as in the upper parts of Figure 13, the microstructure tends to be cellular or cellular-denditric.

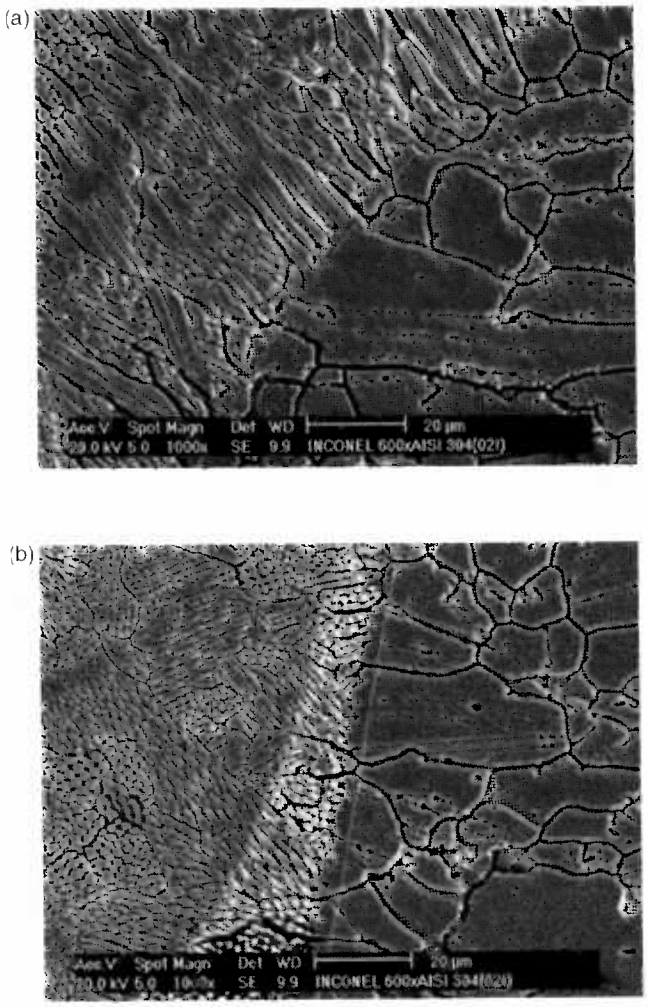

Figure 12. (a) and (b) Images obtained by ESM for the interface between the WZ and the Inconel 600.

In the case of the interface with the stainless steel, the WZ solidifies into ferrite dendrite δ, which is established by higher levels of chrome and iron in this region, as shown in Figure 7(b) and in Table 1. The nickel is rejected by the liquid, establishing formation of an austenitic solid phase (γ). There is a solid state reaction from ferrite δ to austenite-γ, but there is still a small level of residual δ at environmental temperature. The presence of ferrite-δ indicated in Figure 13 is associated with the higher percentage of chrome in the matrix measured by EDX, facilitating the stabilization of this meta-stable phase at environmental temperature. In the interface between the WZ and the Inconel, solidification proceeds by means of growth in austenitic dendrites, which is stabilized by the high level of nickel in this region, as shown in Figure 7(b). Therefore, the WZ only consists of an austenitic phase in the regions close to the interface with the Inconel, and close to the interface with the stainless steel, there may be ferrite δ.

After the epitaxial growth, the advance speed of the S-L interface (R) retains a practically constant value[14], while modifications in the temperature gradient and in the chemical composition cause alterations in the solidification morphology. The size of the cell or the dendrite is

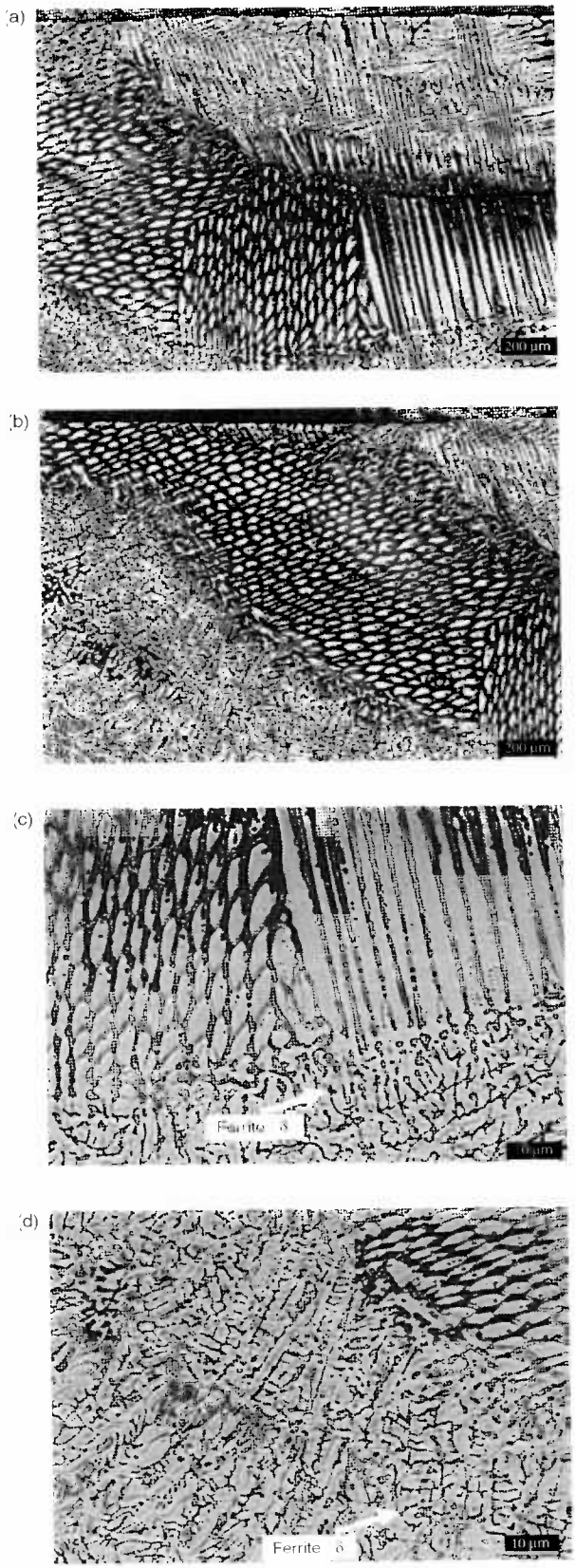

Figure 13. Images obtained under an MO for the WZ showing areas of transition with diverse morphologies (a) predominantly cellular with a small dendritic region in the lower part, (b) dendritic (lower region) and cellular (upper region), (c) dendritic (lower region) and cellular (upper region) and (d) predominantly dendritic, with a cellular region in the top right area.

Table 2. Mechanical properties of the welds between the AISI 304 steel and the Inconel 600.

Sample	Maximam load (kgf)	Deformation (%)	Weld efficiency (%)
AISI 304	687.9 ± 1.2	89.6 ± 1.5	–
Inconel 600	694.1 ± 0.7	57.7 ± 0.8	–
Junta AISI 304/ Inconel 600	617.9 ± 7.7	37.5 ± 1.5	89.8 ± 1.1

determined by the *G*/*R* ratio (cooling speed). Figure 15 shows a fine microstructure with cell or dendrite spacing close to 30 μm.

Another factor that alters the morphology of the WZ is the effect caused by the laser pulse over the area of incidence of the previous pulse. The 30% overlapping of the pulses, as seen in Figure 8(c),(d), causes changes in the WZ solidification morphology. The alterations to the morphology and size of the cells or dendrites can be seen in Figure 13. The reheating causes alterations in the *G* and *R* parameters and in the local chemical composition. The microstructure of the overlapped laser region is reheated and rewelded, and it can be seen that the morphology changes from dendritic to cellular-dendritic, indicating a higher cooling speed in this region.

Some of the mechanical properties obtained from the tensile tests are shown in Table 2. This table shows the maximum load supported by the welded joint, the maximum load supported by the BMs, deformation and weld effectiveness. According to Souza[21], the breaking load is the value that has to be recorded in welds that have discontinuities. The efficiency of the weld can be measured in percentage terms, based on the ratio between the maximum load supported by the welded joint and the maximum load supported by the BMs with the lowest resistance. The maximum load supported by the BM with the lowest mechanical resistance, which is AISI 304 steel, is 687.9 kgf (6879 N) and the maximum breaking strain of the joint is 617.9 kgf (6179 N), as seen in Table 2. Therefore, the welding efficiency in these conditions is close to 90%. The deformation of the welded joint has a value lower than that obtained for the BMs, as a consequence of the presence of pores and other possible undetected discontinuities, as well as the presence of a rough fusion structure.

Vickers microhardness measurements taken in the WZ lead to an average value of 205 ± 19 HV. Variations in the chemical composition and solidification morphology do not cause significant variations in the Vickers microhardness profile throughout the cross section of the welded joint.

4. Conclusions

In the conditions used in the laser welding, the penetration depths are practically total and constant. Epitaxial growth can be seen at the start of the WZ, on the AISI 304 steel and Inconel 600 sides.

There is a concentration gradient of the iron and nickel elements in the WZ.

The morphology of the joint solidification is basically denditric and cellular-denditric.

The morphology of WZ solidification is altered by the conditions of cooling, chemical composition and pulse overlapping.

The variation in Vickers microhardness values in the WZ is not high.

In the conditions employed, the welding efficiency is approximately 90%, indicating behaviour similar to that of the BMs.

Acknowledgements

Thanks to the University Centre of FEI for the financial help to grant holder IC André Lotto. To technician MSc. Luis Carlos Elias da Silva and to grant holder Luis Gustavo C. de Oliveira, both of IPEN, for their collaboration in during this work, and to CNPq for their financial support.

Note

1. Email: mdneves@ipen.br

References

1. Berretta JR, Rossi W, Neves MDM, Almeida IA, Wetter NU, Nogueira GEC, Vieira ND Jr. Welding between Inconel 600 and AISI 304 with a pulsed Nd: YAG laser. III COBEF – Brazilian Congress of Manufacturing Engineering; 2005, Joinville, Minutes of III COBEF.
2. Irving B. Lasers continue to penetrate automotive production lines. Weld J. 2000 Jun;79(6):33–36.
3. Tusek J, Kampus Z, Suban M. Welding of tailored blanks of different materials. Mater Process Technol. 2001;(119): 180–184.
4. Metals Handbook. Welding, Brazing & Soldering. 9th ed. Vol. 6. Metals Park (OH): ASM; 1983. p. 647–671.
5. Savage WF, Aronson AH. Preferred orientation in the weld fusion zone. Weld J. 1966;45(2):85s–89s.
6. Savage WF, Nippes EF, Erickson JS. Solidification mechanisms in fusion welds. Weld J. 1976;55(8): 213s–221s.
7. David SA, Vitek JM. Int Mater Rev. 1989;34:213–245.
8. David SA, Babu SS. Mathematical modelling of weld phenomena. In: Cerjak H, Bhadeshia HKDH, editors. Vol. 3. London: The Institute of Materials; 1997. p. 151–180.
9. Kou S. Weld metallurgy. New York: Wiley; 1987.
10. Savage WF. Solidification, segregation and weld imperfections. Weld World. 1980;18(5–6):89–114.
11. Nelson TW, Lippold JCE, Mills MJ. Nature and evolution of the fusion boundary in ferritic-austenitic dissimilar weld metals. Part 1 Weld Res Suppl. 1999; 329s–337s.
12. Chalmers B. Principles of solidification. New York: Wiley; 1967.
13. Flemings MC. Solidification processing. New York: McGraw-Hill Publishing Co; 1974.
14. Lippold JC, Clark WAT, Tumuluru M. An investigation of weld metal interfaces. In: Cieslak MJ, Perepezlo JH, Glicksman ME, editors. The minerals, metals & materials society; 1992. p. 141–145.
15. Kurz Wand Fisher DJ. Fundamentals of solidification. Aedermannsdorf: Trans Tech Publications Inc. 1989.

16. Wang N, Mokadem S, Rappaz M, Kurz W. Solidification cracking of super alloy single and bi-crystals. Act Mater. 2004;52:3173–3182.
17. David SA, Vitek JM, Hebble TL. Effect of rapid solidification on SS weld metal microstructures and its implications on the Schaeffler diagram. Weld J. 1987;289s–300s.
18. Lippold JC. Centreline cracking in deep penetration electron beam welds in type 304L stainless steel. Weld J. 1985;127s–136s.
19. Kim Jae-Do, Kim Cheol-Jung, Chung Chin-Man. Repair welding of etched tubular components of nuclear power plant by Nd: YAG laser. J Mat Proc Tech. 2001;114:51–56.
20. Park KS, Han WJ. Welding characteristics of the Inconel plate using a pulsed Nd: YAG laser beam. J Mat Proc. 2001;113:234–237.
21. Mechanical tests of metal materials – Sérgio Augusto de Souza, Editora Edgard Blucher Ltda, 1982 7th edition – 2000 pages 15–16.